Eur. Phys. J. B **57**, 271–278 (2007)
DOI: 10.1140/epjb/e2007-00179-2

THE EUROPEAN PHYSICAL JOURNAL B

Doping-dependent evolution of low-energy excitations and quantum phase transitions within an effective model for high-T_c copper oxides

M.M. Korshunov[1,2,a] and S.G. Ovchinnikov[1]

[1] L.V. Kirensky Institute of Physics, Siberian Branch of Russian Academy of Sciences, 660036 Krasnoyarsk, Russia
[2] Max-Planck-Institut für Physik komplexer Systeme, 01187 Dresden, Germany

Received 20 March 2007 / Received in final form 21 May 2007
Published online 22 June 2007 – © EDP Sciences, Società Italiana di Fisica, Springer-Verlag 2007

Abstract. In this paper a mean-field theory for the spin-liquid paramagnetic non-superconducting phase of the p- and n-type high-T_c cuprates is developed. This theory applied to the effective $t-t'-t''-J^*$ model with the ab initio calculated parameters and with the three-site correlated hoppings. The static spin-spin and kinematic correlation functions beyond Hubbard-I approximation are calculated self-consistently. The evolution of the Fermi surface and band dispersion is obtained for the wide range of doping concentrations x. For p-type systems the three different types of behavior are found and the transitions between these types are accompanied by the changes in the Fermi surface topology. Thus a quantum phase transitions take place at $x = 0.15$ and at $x = 0.23$.Due to the different Fermi surface topology we found for n-type cuprates only one quantum critical concentration, $x = 0.2$. The calculated doping dependence of the nodal Fermi velocity and the effective mass are in good agreement with the experimental data.

PACS. 74.72.-h Cuprate superconductors (high-T_c and insulating parent compounds) – 74.25.Jb Electronic structure – 73.43.Nq Quantum phase transitions – 71.18.+y Fermi surface: calculations and measurements; effective mass, g factor

1 Introduction

Discovered almost 20 years ago, high-T_c copper oxides still remain a challenge of the modern condensed matter physics. It is not only due to unconventional superconducting state with a highest superconducting transition temperature T_c ever observed. Also they reveal evolution from an undoped antiferromagnetic (AFM) insulator to an almost conventional, though highly correlated [1], Fermi liquid system at the overdoped side of the phase diagram. Between these two regimes the system exhibits strongly correlated, or so-called "pseudogap" metallic behavior up to an optimal doping concentration $x_{opt} \approx 0.16$.

Recent significant improvements of experimental techniques, especially of the Angle-Resolved Photoemission Spectroscopy (ARPES) and the Scanning Tunneling Microscopy (STM), revealed many exciting features of this doping dependent evolution. First of all, the Fermi surface (FS) at low doping concentrations x has been measured [2]. Together with the previous measurements on optimally and overdoped samples (see e.g. review [3] and references therein), these observations provide a unified picture of the doping dependent FS, which changes from the "Fermi arcs" [4] in the underdoped compounds to the "large" Fermi surface in the overdoped systems. Though this change is smooth, it occurs around the optimal doping concentration. Also, the observed evolution is consistent with the Hall coefficient R_H measurements [5].

The pseudogap behavior observed in ARPES is also tracked in the transport measurements. In particular, the resistivity curvature mapping over $T-x$ phase diagram clearly demonstrates crossover between underdoped and overdoped regimes [6]. And the in-plane resistivity ρ_{ab} shows T-linear dependence only around x_{opt}.

The drastic change of the quasiparticle dynamics around the optimal doping was found by the time-resolved measurements of the photoinduced change in reflectivity for $Bi_2Sr_2Ca_{1-y}Dy_yCu_2O_{8+\delta}$ (BSCCO) [7]. Namely, the spectral weight shifts expected for a BCS superconductor can account for the photoinduced response in overdoped, but not underdoped BSCCO. This agrees with the observed difference of the low-frequency spectral weight transfer in normal and superconducting states on under- and over-doped samples [8,9].

Meanwhile, the integral characteristics of the system demonstrate more smooth behavior upon increase of the doping x. The dependence of the chemical potential shift $\Delta\mu$ on x shows pinning at $x < x_{opt}$, and

[a] e-mail: maxim@mpipks-dresden.mpg.de

evolves smoothly at higher doping concentrations [10]. The measured nodal Fermi velocity v_F is almost doping-independent within experimental error of 20% [11,12]. The experiments involving combination of dc transport and infrared spectroscopy revealed an almost constant effective electron mass $m^*/m = 3.8 \pm 2$ in the underdoped and slightly overdoped $La_{2-x}Sr_xCuO_4$ (LSCO) and $YBa_2Cu_6O_y$ (YBCO) [13]. Low-x effective mass dependence contradicts predictions of the Brinkman-Rice metal-insulator transition theory [14], predicting divergence of the m^* at the point of transition. One of the main drawbacks in this theory is that the magnetic correlations were neglected. Thus the discrepancy with the experiment emphasizes the importance of these correlations in high-T_c copper oxides.

From the theoretical point of view, the description of the crossover between almost localized picture and the Fermi liquid regime is very difficult. Starting from the Fermi liquid approach one may discuss the overdoped and, partly, optimally doped region, while for underdoped and undoped samples this approach is not applicable. The strong-coupling Gutzwiller approximation [15] for the Hubbard model provides a good description for the correlated metallic system. This approximation is equivalent [16,17] to the mean-field saddle-point solution within a slave-boson approach [18]. At the same time, as shown within $1/d$ expansion [16], with d being the dimensionality of the lattice, the Gutzwiller approximation is equivalent to the case of $d = \infty$. Obviously, for the quasi-two-dimensional systems such as high-T_c copper oxides this is not a proper limit. The same applies to the Dynamical Mean-Field Theory (DMFT) [19,20], which is exact only for $d = \infty$. In this limit the short-range magnetic fluctuations are excluded. It is not a good starting point for the system with long-range AFM order at low x and short-range AFM correlations in the underdoped region.

To describe the doping dependent evolution of the low-energy excitations we develop a strong-coupling mean-field theory for the paramagnetic non-superconductive phase of high-T_c copper oxides starting from the local limit. To go beyond the usual Hubbard-I approximation a self-consistently calculated static spin-spin and kinematic correlation functions are taken into account. Within this approximation in the framework of the effective $t-t'-t''-J^*$ model with ab initio calculated parameters we obtain a doping-dependent evolution of the FS, effective mass and nodal Fermi velocity. The analysis of the low-energy excitations behavior for p-type cuprates yields two quantum phase transitions associated with the change of the FS topology. For n-type cuprates we observe only single quantum critical concentration. The key aspect in these findings is an adequate description of the electron scattering by the short range magnetic fluctuations accompanied by the three-site correlated hoppings.

The paper is organized as follows. In Section 2 the effective model and the approximations are described. The results of the calculations for p-type cuprates are presented in Section 3. Also, the critical comparison of the $t-t'-t''-J^*$ and $t-t'-t''-J$ models is made, and the role of short range magnetic order is discussed. Section 4 contains results for n-type cuprates. The last section summarize this study, and the main points are discussed.

2 Model and approximations

High-T_c cuprates belong to a class of strongly correlated systems where the standard local density approximation (LDA) schemes and the weak-coupling perturbation theories yield an inappropriate results. To overcome this difficulty recently we have developed an LDA+GTB method [21]. In this method the ab initio LDA calculation is used to construct the Wannier functions and to obtain the single electron and Coulomb parameters of the multiband Hubbard-type model. Within this model the electronic structure in the strong correlation regime is calculated by the Generalized Tight-Binding (GTB) method [22,23]. The latter combines the exact diagonalization of the model Hamiltonian for a small cluster (unit cell) with perturbative treatment of the intercluster hopping and interactions. For undoped and weakly doped LSCO and $Nd_{2-x}Ce_xCuO_4$ (NCCO) this scheme results in a charge transfer insulator with a correct value of the gap and the dispersion of bands in agreement with the experimental ARPES data (see Ref. [21] for details).

Then this multiband Hubbard-type Hamiltonian was mapped onto an effective low-energy model [21]. Parameters of this effective model were obtained directly from the ab initio parameters of the multiband model. The low-energy model appears to be the $t-t'-t''-J^*$ model ($t-t'-t''-J$ model with the three-site correlated hoppings) for n-type cuprates and the *singlet-triplet* $t-t'-t''-J^*$ model for p-type systems. However, for $x < 0.7$ in a phase without a long-range magnetic order the role of the triplet state and the singlet-triplet hybridization is negligible [24]. Therefore, the triplet state could be omitted and in the present paper we will describe the low-energy excitations in the single-layer p- and n-type cuprates within the $t-t'-t''-J^*$ model.

To write down the model Hamiltonian we use the Hubbard X-operators [25]: $X_f^{\alpha} \leftrightarrow X_f^{n,n'} \equiv |n\rangle\langle n'|$. Here index $\alpha \leftrightarrow (n,n')$ enumerates quasiparticle with energy $\omega_\alpha = \varepsilon_n(N+1) - \varepsilon_{n'}(N)$, where ε_n is the nth energy level of the N-electron system. The commutation relations between X-operators are quite complicated, i.e. two operators commute on another operator, not a c-number. Nevertheless, depending on the difference of the number of fermions in states n and n' it is possible to define quasi-Fermi and quasi-Bose type operators in terms of obeyed statistics. In this notations the Hamiltonian of the $t-t'-t''-J^*$ model in the hole representation have the form:

$$H = \sum_{f,\sigma} (\varepsilon_0 - \mu) X_f^{\sigma,\sigma} + \sum_{f \neq g,\sigma} t_{fg} X_f^{\sigma,0} X_g^{0,\sigma} + \sum_{f \neq g} J_{fg} \left(\boldsymbol{S}_f \boldsymbol{S}_g - \frac{1}{4} n_f n_g \right) + H_3. \quad (1)$$

Here μ is the chemical potential, $\boldsymbol{S}_f$ is the spin operator, $S_f^+ = X_f^{\sigma,\bar{\sigma}}$, $S_f^- = X_f^{\bar{\sigma},\sigma}$, $S_f^z = \frac{1}{2}\left(X_f^{\sigma,\sigma} - X_f^{\bar{\sigma},\bar{\sigma}}\right)$, $n_f = \sum_\sigma X_f^{\sigma,\sigma}$ is the number of particles operator, $J_{fg} = 2\tilde{t}_{fg}^2/E_{ct}$ is the exchange parameter, E_{ct} is the charge-transfer gap. In the notations of reference [21] the hopping matrix elements t_{fg} corresponds to t_{fg}^{SS} and $-t_{fg}^{00}$ for p- and n-type cuprates, respectively, and $\tilde{t}_{fg} = t_{fg}^{0S}$. Hamiltonian H_3 contains the three-site interaction terms:

$$H_3 = \sum_{f\neq g\neq m,\sigma} \frac{\tilde{t}_{fm}\tilde{t}_{mg}}{E_{ct}} \left(X_f^{\sigma,0}X_m^{\bar{\sigma},\sigma}X_g^{0,\bar{\sigma}} - X_f^{\sigma,0}X_m^{\bar{\sigma},\bar{\sigma}}X_g^{0,\sigma}\right). \tag{2}$$

There is a simple correspondence between X-operators and single-electron annihilation operators: $a_{f\lambda\sigma} = \sum_\alpha \gamma_{\lambda\sigma}(\alpha)X_f^\alpha$, where the coefficients $\gamma_{\lambda\sigma}(\alpha)$ determines the partial weight of the quasiparticle α with spin σ and orbital index λ. These coefficients are calculated straightforwardly within the GTB scheme. In the considered case there is only one quasi-Fermi-type quasiparticle, $\alpha = (0,\sigma)$, with $\gamma_{\lambda\sigma}(\alpha) = 1$, and the Hamiltonian in the generalized form in momentum representation is given by:

$$H = \sum_{\boldsymbol{k},\sigma} (\varepsilon_0 - \mu)\, X_{\boldsymbol{k}}^{\sigma,\sigma} + \sum_{\boldsymbol{k}}\sum_{\alpha,\beta} t_{\boldsymbol{k}}^{\alpha\beta} X_{\boldsymbol{k}}^{\alpha\dagger} X_{\boldsymbol{k}}^{\beta} + \sum_{\boldsymbol{p},\boldsymbol{q}}\sum_{\alpha,\beta,\sigma,\sigma'} V_{\boldsymbol{pq}}^{\alpha\beta,\sigma\sigma'} X_{\boldsymbol{p}}^{\alpha\dagger} X_{\boldsymbol{p}-\boldsymbol{q}}^{\sigma,\sigma'} X_{\boldsymbol{q}}^{\beta}. \tag{3}$$

Here $t_{\boldsymbol{k}}^{\alpha\beta}$ and $V_{\boldsymbol{pq}}^{\alpha\beta,\sigma\sigma'}$ are Fourier transforms of $\delta_{\alpha\beta}t_{fg}$ and $-\sigma/\sigma'\tilde{t}_{fm}\tilde{t}_{mg}/E_{ct}$, respectively.

The Fourier transform of the two-time retarded Green function in the energy representation, $G_\lambda(\boldsymbol{k},E) = \left\langle\left\langle a_{\boldsymbol{k}\lambda\sigma} \middle| a_{\boldsymbol{k}\lambda\sigma}^\dagger \right\rangle\right\rangle_E$, can be rewritten in terms of the matrix Green function $\left[\hat{D}(\boldsymbol{k},E)\right]_{\alpha\beta} = \left\langle\left\langle X_{\boldsymbol{k}}^\alpha \middle| X_{\boldsymbol{k}}^{\beta\dagger} \right\rangle\right\rangle_E$:

$$G_\lambda(\boldsymbol{k},E) = \sum_{\alpha,\beta} \gamma_{\lambda\sigma}(\alpha)\gamma_{\lambda\sigma}^*(\beta) D^{\alpha\beta}(\boldsymbol{k},E). \tag{4}$$

The diagram technique for Hubbard X-operators has been developed [26,27] and the generalized Dyson equation [28] in the paramagnetic phase ($\langle X_0^{\sigma,\sigma}\rangle = \langle X_0^{\bar{\sigma},\bar{\sigma}}\rangle$) reads:

$$\hat{D}(\boldsymbol{k},E) = \left[\hat{G}_0^{-1}(E) - \hat{P}(\boldsymbol{k},E)\hat{t}_{\boldsymbol{k}} - \hat{P}(\boldsymbol{k},E)\hat{V}_{\boldsymbol{kk}}^{\sigma\sigma}\langle X_0^{\sigma,\sigma}\rangle + \hat{\Sigma}(\boldsymbol{k},E)\right]^{-1}\hat{P}(\boldsymbol{k},E). \tag{5}$$

Here, $\hat{G}_0^{-1}(E)$ is the exact local Green function, $G_0^{\alpha\beta}(E) = \delta_{\alpha\beta}/\left[E - (\varepsilon_n - \varepsilon_{n'})\right]$, $\hat{\Sigma}(\boldsymbol{k},E)$ and $\hat{P}(\boldsymbol{k},E)$ are the self-energy and the strength operators, respectively. The presence of the strength operator is due to the redistribution of the spectral weight between the Hubbard subbands, that is an intrinsic feature of the strongly correlated electron systems. It also should be stressed that $\hat{\Sigma}(\boldsymbol{k},E)$ in equation (5) is the self-energy in X-operators representation and therefore it differs from the self-energy entering Dyson equation for the weak coupling perturbation theory for $G_\lambda(\boldsymbol{k},E)$.

Within Hubbard-I approximation [29] the self-energy $\hat{\Sigma}(\boldsymbol{k},E)$ is equal to zero and the strength operator $\hat{P}(\boldsymbol{k},E)$ is replaced by $P^{\alpha\beta}(\boldsymbol{k},E) \to P^{\alpha\beta} = \delta_{\alpha\beta}F_\alpha$, where $F_{\alpha(n,n')} = \left\langle X_f^{n,n}\right\rangle + \left\langle X_f^{n',n'}\right\rangle$ is the occupation factor.

Taking into account that in the considered paramagnetic phase $\left\langle X_f^{\sigma,\sigma}\right\rangle = (1-x)/2$, $\left\langle X_f^{0,0}\right\rangle = x$, with x being the doping concentration, after all substitutions and treating all $\boldsymbol{k}$-independent terms as the chemical potential renormalization, the generalized Dyson equation for the Hamiltonian (1) becomes:

$$D(\boldsymbol{k},E) = \left[E - (\varepsilon_0 - \mu) - \frac{1+x}{2}t_{\boldsymbol{k}} - \frac{1+x}{2}\frac{\tilde{t}_{\boldsymbol{k}}^2}{E_{ct}}\frac{1-x}{2} + \Sigma(\boldsymbol{k},E)\right]^{-1}\frac{1+x}{2}. \tag{6}$$

To go beyond the Hubbard-I approximation we have to calculate $\Sigma(\boldsymbol{k},E)$. For this purpose we use an equations of motion method for the X-operators [30]. The exact equation of motion for X_k^α is:

$$i\dot{X}_{\boldsymbol{k}}^\alpha = [X_{\boldsymbol{k}}^\alpha, H] = (\varepsilon_0 - \mu)X_{\boldsymbol{k}}^\alpha + L_{\boldsymbol{k}}^\alpha = (\varepsilon_0 - \mu)X_{\boldsymbol{k}}^\alpha + L_{\boldsymbol{k}}^{\alpha(0)} + (L_{\boldsymbol{k}}^\alpha - L_{\boldsymbol{k}}^{\alpha(0)}). \tag{7}$$

Here $L_{\boldsymbol{k}}^{\alpha(0)}$ is the linearized and decoupled in Hubbard-I approximation operator $L_{\boldsymbol{k}}^\alpha$,

$$L_{\boldsymbol{k}}^{\alpha(0)} = \frac{1+x}{2}t_{\boldsymbol{k}} + \frac{1+x}{2}\frac{\tilde{t}_{\boldsymbol{k}}^2}{E_{ct}}\frac{1-x}{2}. \tag{8}$$

Let us define $\tilde{L}_{\boldsymbol{k}}^\alpha = L_{\boldsymbol{k}}^\alpha - L_{\boldsymbol{k}}^{\alpha(0)}$ and linearize it with respect to $X_{\boldsymbol{k}}^\alpha$:

$$\tilde{L}_{\boldsymbol{k}}^\alpha = \sum_\beta T_{\boldsymbol{k}}^{\alpha\beta} X_{\boldsymbol{k}}^\beta + \tilde{L}_{\boldsymbol{k}}^{\alpha(irr)}, \tag{9}$$

where $T_{\boldsymbol{k}}^{\alpha\beta} = \frac{\left\langle\left\{\tilde{L}_{\boldsymbol{k}}^\alpha, X_{\boldsymbol{k}}^{\beta\dagger}\right\}\right\rangle}{\left\langle\left\{X_{\boldsymbol{k}}^\beta, X_{\boldsymbol{k}}^{\beta\dagger}\right\}\right\rangle}$ are the coefficients of the linearization. All effects of the finite quasiparticle lifetime are contained in the irreducible part $\tilde{L}_{\boldsymbol{k}}^{\alpha(irr)}$. In this paper we neglect it, $\tilde{L}_{\boldsymbol{k}}^{\alpha(irr)} \to 0$.

Since the exact equation for the Green function is given by $E\left\langle\left\langle X_{\boldsymbol{k}}^\alpha \middle| X_{\boldsymbol{k}}^{\beta\dagger}\right\rangle\right\rangle_E = \left\langle\left\{X_{\boldsymbol{k}}^\alpha, X_{\boldsymbol{k}}^{\beta\dagger}\right\}\right\rangle + \left\langle\left\langle i\dot{X}_{\boldsymbol{k}}^\alpha \middle| X_{\boldsymbol{k}}^{\beta\dagger}\right\rangle\right\rangle_E$, it is straightforward to find that in our approximation $T_{\boldsymbol{k}}^{\alpha\beta}$ corresponds to the static part of the self-energy:

$$\hat{\Sigma}(\boldsymbol{k}) = -\hat{T}_{\boldsymbol{k}}. \tag{10}$$

Introducing notations for the static spin-spin correlation functions

$$C_{\boldsymbol{q}} = \sum_{f,g} e^{-i(f-g)\boldsymbol{q}} \left\langle X_f^{\sigma,\bar{\sigma}} X_g^{\bar{\sigma},\sigma}\right\rangle = 2\sum_{\boldsymbol{r}} e^{-i\boldsymbol{r}\boldsymbol{q}} \langle S_{\boldsymbol{r}}^z S_0^z\rangle, \tag{11}$$

and for the kinematic correlation functions

$$K_{\boldsymbol{q}} = \sum_{f,g} e^{-i(f-g)\boldsymbol{q}} \left\langle X_f^{\sigma,0} X_g^{0,\sigma} \right\rangle, \tag{12}$$

the expression for the quasiparticle self-energy becomes:

$$\Sigma(\boldsymbol{k}) = \frac{2}{1+x}\frac{1}{N}\sum_{\boldsymbol{q}} \left[Y_1(\boldsymbol{k},\boldsymbol{q}) K_{\boldsymbol{q}} - Y_2(\boldsymbol{k},\boldsymbol{q})\frac{3}{2} C_{\boldsymbol{q}} \right]. \tag{13}$$

Here N is the number of vectors in momentum space, and coefficients $Y_1(\boldsymbol{k},\boldsymbol{q})$ and $Y_2(\boldsymbol{k},\boldsymbol{q})$ are given by the following expressions:

$$Y_1(\boldsymbol{k},\boldsymbol{q}) = t_{\boldsymbol{q}} - \frac{1-x}{2} J_{\boldsymbol{k}-\boldsymbol{q}} - x\frac{\tilde{t}_{\boldsymbol{q}}^2}{E_{ct}} - \frac{1+x}{2}\frac{2\tilde{t}_{\boldsymbol{k}}\tilde{t}_{\boldsymbol{q}}}{E_{ct}},$$

$$Y_2(\boldsymbol{k},\boldsymbol{q}) = t_{\boldsymbol{k}-\boldsymbol{q}} - \frac{1-x}{2}\left(J_{\boldsymbol{q}} - \frac{\tilde{t}_{\boldsymbol{k}-\boldsymbol{q}}^2}{E_{ct}} \right) - \frac{1+x}{2}\frac{2\tilde{t}_k\tilde{t}_{\boldsymbol{k}-\boldsymbol{q}}}{E_{ct}}.$$

Until now we have made two major approximations. First, we neglected irreducible part of the self-energy, $\tilde{L}_{\boldsymbol{k}}^{\alpha(irr)}$, thus allowing quasiparticles to have infinite lifetime. Second, the strength operator $\hat{P}(\boldsymbol{k},E)$ is taken in the zero-loop approximation within the X-operator's diagram technique, $P^{\alpha\beta}(\boldsymbol{k},E) \approx \delta_{\alpha\beta}(1+x)/2$. This form of the strength operator is the same as in the Hubbard-I decoupling in the equation of motion method. Deviation of the strength operator from unity reflects very important feature of the strongly correlated systems, namely the redistribution of the spectral weight between the Hubbard subbands. Previously [31], results of the Hubbard-I approximation to the half-filled two-dimensional Hubbard model assuming a long range AFM order at low temperature were compared to the Quantum Monte-Carlo (QMC) data [32]. It occurs that calculated spectral functions and the redistribution of the spectral weight are in a qualitative agreement with the QMC results. This could justify the application of the zero-loop approximation in present paper where we are dealing with the short range AFM fluctuations. The corrections beyond the zero-loop approximation lead to the finite quasiparticle lifetime [26]. Note, since we use the perturbation theory with hopping t and exchange J as small parameters, the corrections to the obtained results will be small to the extent of smallness of the higher powers of t/E_{ct} and J/E_{ct}.

Kinematic correlation functions (12) were calculated straightforwardly via spectral theorem to obtain $\left\langle X_f^{\sigma 0} X_g^{0\sigma} \right\rangle$ using Green function (6):

$$\left\langle\left\langle X_{\boldsymbol{k}}^{0,\sigma} \middle| X_{\boldsymbol{k}}^{\sigma 0} \right\rangle\right\rangle_E = \frac{(1+x)/2}{E - (\varepsilon_0 - \mu) - \frac{1+x}{2} t_{\boldsymbol{k}} - \frac{1-x^2}{4}\frac{\tilde{t}_{\boldsymbol{k}}^2}{E_{ct}} + \Sigma(\boldsymbol{k})}. \tag{14}$$

The spin-spin correlation functions for the $t-J$ model with three-site correlated hoppings H_3 were calculated in reference [33]. In that paper the equations of motion for the spin-spin Green function $\left\langle\left\langle X_f^{\sigma\bar{\sigma}} \middle| X_g^{\bar{\sigma}\sigma} \right\rangle\right\rangle_\omega$ were decoupled in the rotationally invariant quantum spin liquid phase, similar to references [34,35]. The results of this approach for a static magnetic susceptibility for the $t-J$ model are similar to those obtained by other methods [36,37]. Higher-order correlation functions appearing due to the H_3 term are decoupled in the following way:

$$\left\langle\left\langle X_m^{\bar{\sigma}\bar{\sigma}} X_n^{\sigma 0} X_l^{0\bar{\sigma}} \mid X_j^{\bar{\sigma}\sigma} \right\rangle\right\rangle_\omega \to \left\langle X_m^{\bar{\sigma}\bar{\sigma}} \right\rangle \left\langle\left\langle X_n^{\sigma 0} X_l^{0\bar{\sigma}} \mid X_j^{\bar{\sigma}\sigma} \right\rangle\right\rangle_\omega$$

$$\left\langle\left\langle X_m^{\sigma\bar{\sigma}} X_l^{\sigma 0} X_n^{0\sigma} \mid X_j^{\bar{\sigma}\sigma} \right\rangle\right\rangle_\omega \to \left\langle X_l^{\sigma 0} X_n^{0\sigma} \right\rangle \left\langle\left\langle X_m^{\sigma\bar{\sigma}} \mid X_j^{\bar{\sigma}\sigma} \right\rangle\right\rangle_\omega.$$

Thus, higher-order kinematic and spin-spin scattering channels are decoupled.

After the terms proportional to $x\left(2\tilde{t}_{01}/E_{ct}\right)^2$ being neglected, the expression for Fourier transform of the spin-spin Green function becomes:

$$\left\langle\left\langle X_{\boldsymbol{q}}^{\sigma,\bar{\sigma}} \mid X_{\boldsymbol{q}}^{\bar{\sigma},\sigma} \right\rangle\right\rangle_\omega = \frac{A_{\boldsymbol{q}}(\omega)}{\omega^2 - \omega_{\boldsymbol{q}}^2}, \tag{15}$$

where

$$A_{\boldsymbol{q}}(\omega) = \frac{1}{N}\sum_{\boldsymbol{k}} \left[\left(-2t_{\boldsymbol{k}} + \frac{1-x}{2}\frac{\tilde{t}_k^2}{E_{ct}} \right)(K_{\boldsymbol{k}} - K_{\boldsymbol{q}-\boldsymbol{k}}) + 4J_{\boldsymbol{k}}\left(C_{\boldsymbol{q}-\boldsymbol{k}} - C_{\boldsymbol{k}}\right) \right], \tag{16}$$

and magnetic excitations spectrum $\omega_{\boldsymbol{q}}$ represented by equation (26) of paper [33].

The following results were obtained by self-consistent calculation of the chemical potential μ, the spin-spin correlation functions (11) using Green function (15), and the kinematic correlation functions (12) using Green function (14) with the self-energy (13).

3 Results for p-type cuprates

For LSCO the LDA+GTB calculated parameters are (in eV): $t \equiv t_{01} = 0.93$, $t' \equiv t_{11} = -0.12$, $t'' \equiv t_{02} = 0.15$, $J \equiv J_{01} = 0.295$, $J' \equiv J_{11} = 0.003$, $J'' \equiv J_{02} = 0.007$, $\tilde{t}_{01} = 0.77$, $\tilde{t}_{11} = -0.08$, $\tilde{t}_{02} = 0.12$, and $E_{ct} = 2$. All figures below are in electron representation.

First of all we would like to stress the important effects caused by the three-site correlated hoppings H_3 and the renormalizations due to the short range magnetic order. Previously, the importance of the three-site correlated hoppings in the normal and superconducting phases has been demonstrated in references [33,38,39]. In Figure 1 we present our results for 16% hole doping within different approximations. Evidently, introduction of three-site interaction terms results in the change of the position of the top of the valence band. Therefore, this will become important at small x. In AFM phase of the $t-J$ model there is a symmetry around $(\pi/2,\pi/2)$ point. In the paramagnetic phase this symmetry is absent. Due to the scattering on the short range magnetic fluctuations with AFM wave vector $\boldsymbol{Q} = (\pi,\pi)$ the states near the (π,π) point are pushed below the Fermi level (see Fig. 1), thus totally changing the shape of the FS. In other words, the

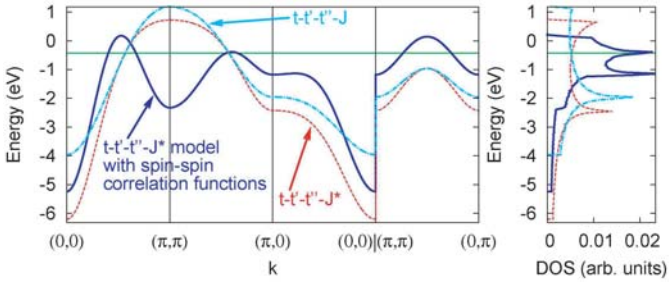

Fig. 1. (Color online) The quasiparticle dispersion (on the left) and the density of states (DOS, on the right) in the paramagnetic phase of p-type cuprate with $x = 0.16$. The position of the chemical potential is denoted by the horizontal (green) line. Results within the Hubbard-I approximation are shown by dashed (red) and dash-dotted (cyan) curves for the model with ($t-t'-t''-J^*$ model) and without ($t-t'-t''-J$ model) three-site correlated hoppings, respectively. Bold solid (blue) curves represent the results for the $t-t'-t''-J^*$ model with the short range magnetic order.

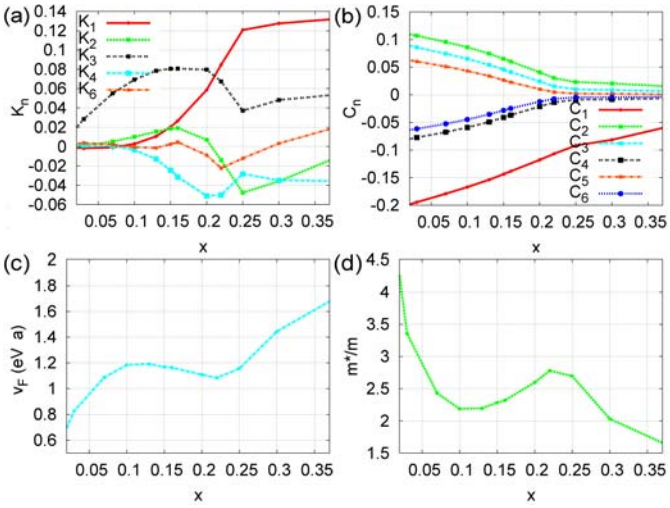

Fig. 2. (Color online) Doping dependent evolution of the kinematic (a) and spin-spin (b) correlation functions within the $t-t'-t''-J^*$ model for p-type cuprates. Index n enumerates real space vectors connecting neighboring sites: $n = 1$ for nearest-neighbors, $n = 2$ for the next nearest neighbors, and so on.In (c) and (d) the doping dependence of the nodal Fermi velocity (in units of eV·a with a being a lattice constant) and the effective mass are shown.

short range magnetic order "tries" to restore the symmetry around $(\pi/2, \pi/2)$ point. In our calculations the short range magnetic fluctuations are taken into account via the spin-spin correlation functions (11).

Our results for the doping dependence of the kinematic and spin-spin correlation functions are shown in Figure 2. Note, the kinematic correlation functions K_n possess a very nontrivial doping dependence. For low concentrations, $x < 0.15$, due to the strong magnetic correlations the hoppings to the nearest and to the next-nearest neighbors are suppressed leading to the small values of K_1 and K_2, while K_3 is not suppressed. Upon increase of the doping concentration above $x \approx 0.15$, magnetic correlations

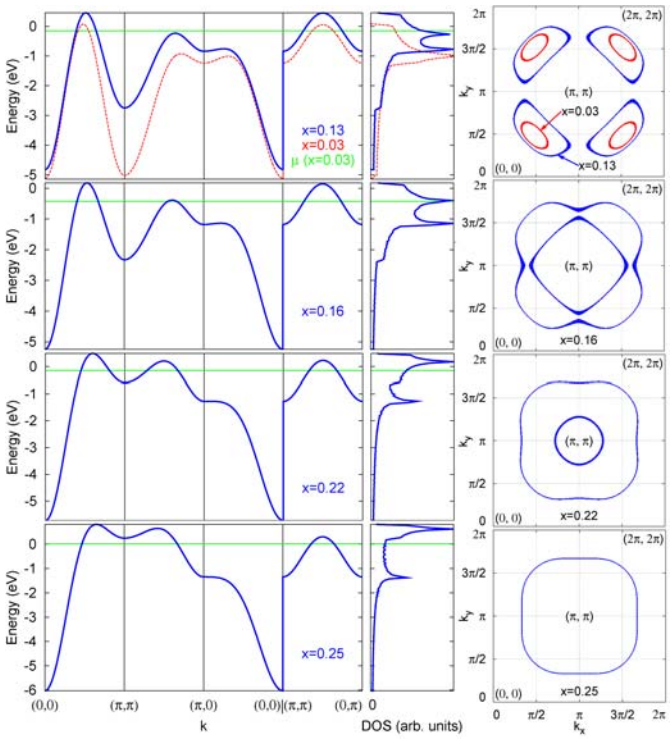

Fig. 3. (Color online) Band structure (on the left), density of states (in the middle), and Fermi surface (on the right) evolution with doping concentration x within the $t-t'-t''-J^*$ model for p-type cuprates.

decrease considerably and nearest-neighbor kinematic correlation function K_1 increase. Next major change sets at $x \approx 0.23$ when the system possesses almost Fermi liquid behavior: K_1 becomes largest of all K_n's, while the magnetic correlation functions C_n and the kinematic correlation function K_3 are strongly suppressed.

So, we can clearly define two points of the crossover, namely $x \approx 0.15$ and $x \approx 0.23$. The system behavior is quite different on the different sides of these points, although there is no phase transition with symmetry breaking occurs. To understand the nature of these crossovers we consider the FS evolution with doping concentration, presented in Figure 3. At low x the FS has the form of the hole pockets centered around $(\pm\pi/2, \pm\pi/2)$ point. Then these pockets enlarge and at $x = 0.15$ all of them merge together, forming the two FS contours. Up to $x = 0.23$ the FS topologically equivalent to the two concentric circles with the central one shrinking toward $(0, 0)$ point. For $x = 0.23$ the central FS contour shrinks to the single point and vanishes, leaving one large hole-type FS.

Apparently, the topology of the FS changes drastically upon doping. In particular, it happens at $x = 0.15$ and at $x = 0.23$. For the first time the "electronic transition" accompanying the change in the FS topology, or the so-called Lifshitz transition, was described in reference [40]. Now such transitions referred as a quantum phase transitions with a co-dimension = 1 (see e.g. paper [41]). Note, when the FS topology changes at quantum critical concentrations $x_1 = 0.15$ and at $x_2 = 0.23$ the density of states at

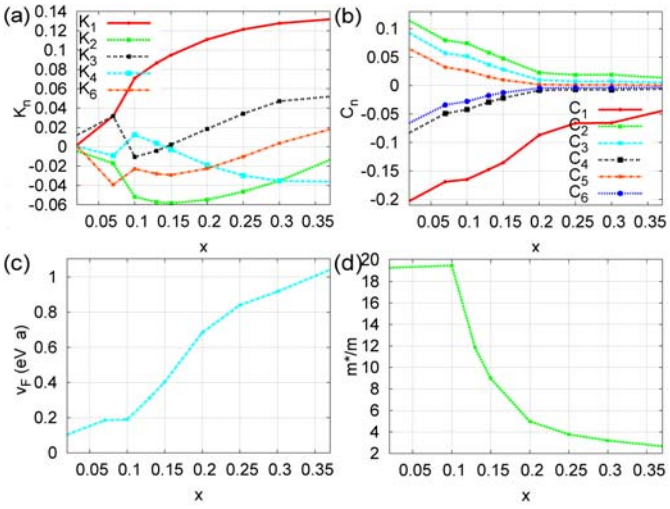

Fig. 4. (Color online) The same as in Figure 2, but within the model for p-type cuprates without three-site correlated hoppings ($t - t' - t'' - J$ model).

the Fermi level also exhibit significant modifications. This results in the different behavior of the kinematic and magnetic correlation functions on the different sides of these crossover points. And the changes in the density of states at the Fermi level will also result in the significant changes of such observable physical quantities as the resistivity and the specific heat.

Also, from the obtained quasiparticle dispersion we calculated the doping dependence of the nodal Fermi velocity v_F and the effective mass m^*/m (see Figs. 2c and 2d). Nodal Fermi velocity does not show steep variations with increase of the doping concentration in agreement with the ARPES experiments [11,12]. Effective mass m^* increase with decreasing x and reveals tendency to the localization in the vicinity of the metal-insulator transition. But this increase is not very large and overall m^*/m doping dependence agrees quite well with the experimentally observed one [13]. Note, the non-monotonic doping dependence of both these quantities reflects the presence of the critical concentrations x_1 and x_2.

To analyze the effect of the three-site hopping term H_3 we also calculated the doping dependence of the band structure and FS within the $t-t'-t''-J$ model. The behavior of the kinematic and the spin-spin correlation functions, presented in Figure 4, is quite different from that of the $t - t' - t'' - J^*$ model. There is only one quantum critical point at $x \approx 0.08$ and the effective mass becomes very large for x approaching zero. For $x > 0.1$ the evolution of the FS and density of states near the Fermi level is smooth, without significant changes (see Fig. 5). Most part of the difference to the $t - t' - t'' - J^*$ model stems from the role of H_3 in the energy of states near the (π, π) point, thus determining the topology of the FS and the physics at low doping concentrations (see Fig. 1).

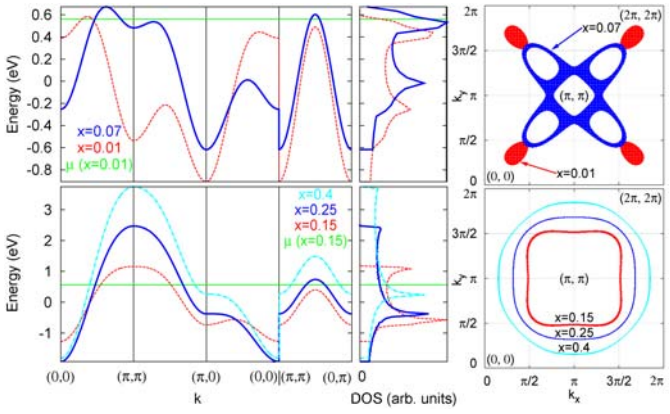

Fig. 5. (Color online) The same as in Figure 3, but within the model for p-type cuprates without three-site correlated hoppings ($t - t' - t'' - J$ model).

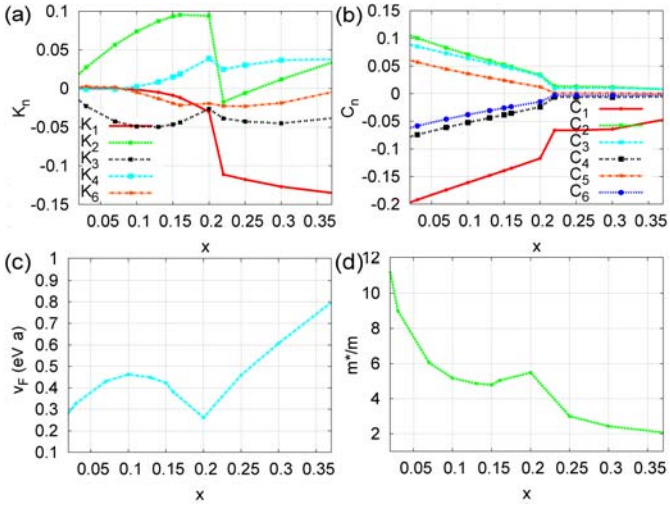

Fig. 6. (Color online) The same as in Figure 2, but within the $t - t' - t'' - J^*$ model for n-type cuprates.

4 Results for n-type cuprates

Now let us consider n-type cuprates within the $t - t' - t'' - J^*$ model. For NCCO the LDA+GTB calculated parameters are (in eV): $t \equiv t_{01} = -0.50$, $t' \equiv t_{11} = 0.02$, $t'' \equiv t_{02} = -0.07$, $J \equiv J_{01} = 0.195$, $J' \equiv J_{11} = 0.001$, $J'' \equiv J_{02} = 0.004$, $\tilde{t}_{01} = -0.63$, $\tilde{t}_{11} = 0.04$, $\tilde{t}_{02} = -0.09$, and $E_{ct} = 2$.

The obtained doping dependence of the kinematic and magnetic correlation functions presented in Figure 6. There is only one crossover point at $x \approx 0.2$. Also, in contrast to the p-type results, the most important kinematic correlation function on the left of this point is K_2, rather than K_3. For $x > 0.2$ the system demonstrates Fermi liquid-like behavior with magnitude of kinematic correlation function decreasing with the distance, and small values of the magnetic correlations.

The role of the short range magnetic order and three-site hopping terms in n-type cuprates is similar to that of p-type. In particular, due to the scattering on the magnetic excitations the states near the (π, π) point pushed

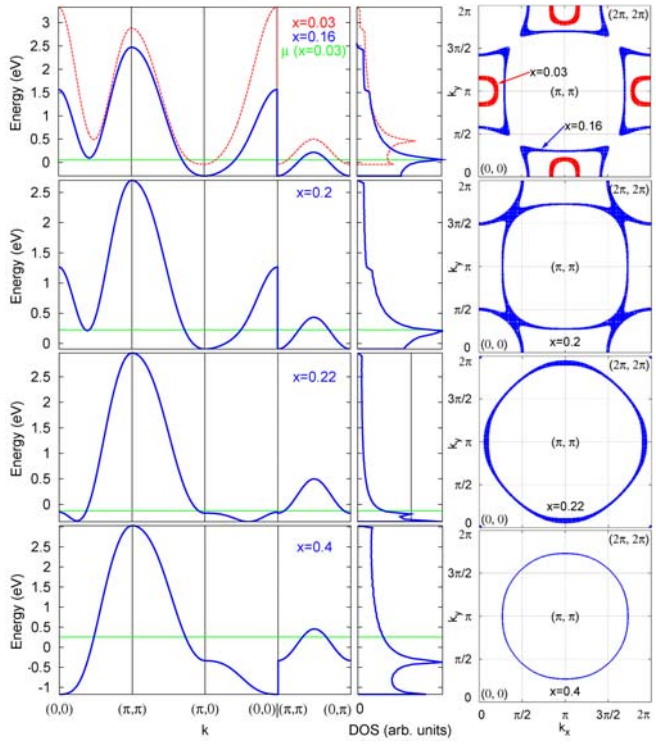

Fig. 7. (Color online) The same as in Figure 3, but within the $t - t' - t'' - J^*$ model for n-type cuprates.

above the Fermi level, and the local symmetry around the $(\pi/2, \pi/2)$ points is restored, reminding of the short-range AFM fluctuations (see Fig. 7).

Instead of hole pockets around the $(\pm\pi/2, \pm\pi/2)$ point in p-type, here at low x the electron pockets around $(\pm\pi, 0)$ and $(0, \pm\pi)$ points are present. Upon increase of the doping concentration these pockets become larger and merge together at $x = 0.2$. For higher concentrations the FS appear to be a large hole-like one, shrinking toward (π, π) point. Therefore, no other changes in the FS topology other than at $x = 0.2$ are present. Referring to the same arguments as in previous section, we claim that in our approach there is only one quantum critical point at $x_n = 0.2$ in the n-type cuprates. The non-monotonic change of the effective mass and the nodal Fermi velocity is also present at this concentration, as evident from Figures 6c and 6d.

5 Discussion and summary

To summarize, we have investigated the doping-dependent evolution of the low-energy excitations for p- and n-type high-T_c cuprates in the regime of strong electron correlations within the sequentially derived effective model with the ab initio parameters. We show that due to the changes of the Fermi surface topology with doping the system exhibits drastic change of the low-energy physics. Namely, for p-type cuprates there exist two critical concentrations, $x_1 \approx 0.15$ and $x_2 \approx 0.23$. Along the different sides of these concentrations the behavior of the density of states near the Fermi level, of the kinematic and magnetic correlation functions, of the effective mass and the nodal Fermi velocity, is drastically different. This let us speak about crossover, or, taking into account the accompanying FS topology changes, about quantum phase transitions at these quantum critical concentrations.

For n-type cuprates due to the specific FS topology we obtain only one quantum critical concentration, $x_n \approx 0.2$.

First of all, we would like to comment on the approximations made in this work. Since we use the perturbation theory with hopping t and exchange J as small parameters, appropriate for the strongly correlated regime, the real part of the corrections to the results obtained will be small to the extent of smallness of the higher powers of t/E_{ct} and J/E_{ct}. This will result in the small changes of the band dispersion and in the fine details of the FS, not changing anything qualitatively.

More concerns give the imaginary part of the neglected corrections to the strength operator $\hat{P}(\boldsymbol{k}, E)$ and to the self-energy $\hat{\Sigma}(\boldsymbol{k}, E)$ through $\tilde{L}_{\boldsymbol{k}}^{\alpha(irr)}$. Application of the equation of motion decoupling method to the Hubbard model with finite quasiparticle lifetime [42,43] reveals that the results of the mean-field-like approximation is qualitatively correct. Quantitatively, at low doping the imaginary part of the self-energy leads to the hiding of the FS portions above the antiferromagnetic Brillouin zone ($(\pi, 0) - (0, \pi)$ line). This results in Fermi arc rather than hole pockets at $x < x_{opt}$ (see Fig. 3). Also, we can compare our results to the numerical methods, namely, to the exact diagonalization studies [44]. The quasiparticle dispersion of the $t - t' - J$ model in reference [44] can be considered as consisting of two bands. For p-type cuprates intensities of the spectral peaks corresponding to the band situated mostly above the Fermi level (in electron representation) are very low. This band is often called a "shadow" band and appears due to the scattering on the short range AFM fluctuations. Notably, our band dispersion from Figures 3 and 7 reproduce very well the shape of the other, "non-shadow", band. It is this band where the most part of the spectral weight is residing, thus determining most of the low-energy properties, except for such subtle effects as a so-called "kink" in dispersion [11].

ARPES experiments reveal that the quasiparticles are strongly suppressed away from the Fermi level. Thus the "effective" bandwidth extracted from ARPES is much smaller than that in the mean-field-type theory. The fact that we neglected imaginary part of strength operator and the self-energy does not allow us to make direct comparison of the calculated band dispersion with the ARPES data. Note, the calculated bands are not one electron bands but a complicated quasiparticle bands carrying a non-integer spectral weight.

Also, all renormalizations not included in consideration will change the values of the critical concentrations x_1, x_2, and x_n. Comparing with the results of a more rigorous theory in paper [42,43], we expect these values to decrease.

Thus we conclude that our theory captures the most important part of the low-energy physics within the

considered (and justified for cuprates) model. This claim is supported by the qualitative agreement with the critical concentrations of crossover observed in the transport experiments [5,6] and in the optical experiment [7–9], and even quantitative agreement of the doping dependence of the nodal Fermi velocity and of the effective mass [11–13]. Although we use a simple mean-field theory, though strong-coupled, the agreement with the experiments is not surprising since we included all necessary for high-T_c copper oxides ingredients. Namely, the short range magnetic order and three-site correlated hoppings. Former is the intrinsic property of the cuprates exhibiting long range AFM order at low x, while latter results from the sequential derivation of the low-energy effective model.

We would like to thank I. Eremin, P. Fulde, N.M. Plakida, A.V. Sherman, and V.Yu. Yushankhai for useful discussions, D.M. Dzebisashvili and V.V. Val'kov for critical reading of the manuscript. Authors acknowledge support form INTAS (YS Grant 05-109-4891), Siberian Branch of RAS (Lavrent'yev Contest for Young Scientists), RFBR (Grants 06-02-16100, 06-02-90537-BNTS), Program of Physical Branch of RAS "Strongly correlated electron systems", and Joint Integration Program of Siberian and Ural Branches of RAS N.74.

References

1. S. Nakamae, K. Behnia, N. Mangkorntong, M. Nohara, H. Takagi, S.J.C. Yates, N.E. Hussey, Phys. Rev. B **68**, 100502(R) (2003)
2. K.M. Shen, F. Ronning, D.H. Lu, F. Baumberger, N.J.C. Ingle, W.S. Lee, W. Meevasana, Y. Kohsaka, M. Azuma, M. Takano, H. Takagi, Z.-X. Shen, Science **307**, 901 (2005)
3. A. Damascelli, Z. Hussain, Z.-X. Shen, Rev. Mod. Phys. **75**, 473 (2003)
4. T. Yoshida, X.J. Zhou, T. Sasagawa, W.L. Yang, P.V. Bogdanov, A. Lanzara, Z. Hussain, T. Mizokawa, A. Fujimori, H. Eisaki, Z.-X. Shen, T. Kakeshita, S. Uchida, Phys. Rev. Lett. **91**, 027001 (2003)
5. Y. Ando, Y. Kurita, S. Komiya, S. Ono, K. Segawa, Phys. Rev. Lett. **92**, 197001 (2004)
6. Y. Ando, S. Komiya, K. Segawa, S. Ono, Y. Kurita, Phys. Rev. Lett. **93**, 267001 (2004)
7. N. Gedik, M. Langner, J. Orenstein, S. Ono, Y. Abe, Y. Ando, Phys. Rev. Lett. **95**, 117005 (2005)
8. A.F. Santander-Syro, R.P.S.M. Lobo, N. Bontemps, W. Lopera, D. Girata, Z. Konstantinovic, Z.Z. Li, H. Raffy, Phys. Rev. B **70**, 134504 (2004)
9. F. Carbone, A.B. Kuzmenko, H.J.A. Molegraaf, E. van Heumen, V. Lukovac, F. Marsiglio, D. van der Marel, K. Haule, G. Kotliar, H. Berger, S. Courjault, P.H. Kes, M. Li, Phys. Rev. B **74**, 064510 (2006)
10. N. Harima, J. Matsuno, A. Fujimori, Y. Onose, Y. Taguchi, Y. Tokura, Phys. Rev. B **64**, 220507(R) (2001)
11. X.J. Zhou, T. Yoshida, A. Lanzara, P.V. Bogdanov, S.A. Kellar, K.M. Shen, W.L. Yang, F. Ronning, T. Sasagawa, T. Kakeshita, T. Noda, H. Eisaki, S. Uchida, C.T. Lin, F. Zhou, J.W. Xiong, W.X. Ti, Z.X. Zhao, A. Fujimori, Z. Hussain, Z.-X. Shen, Nature **423**, 398 (2003)
12. A.A. Kordyuk, S.V. Borisenko, A. Koitzsch, J. Fink, M. Knupfer, H. Berger, Phys. Rev. B **71**, 214513 (2005)
13. W.J. Padilla, Y.S. Lee, M. Dumm, G. Blumberg, S. Ono, K. Segawa, S. Komiya, Y. Ando, D.N. Basov, Phys. Rev. B **72**, 060511(R) (2005)
14. W.F. Brinkman, T.M. Rice, Phys. Rev. B **2**, 4302 (1970)
15. M.C. Gutzwiller, Phys. Rev. Lett. **10**, 159 (1963); M.C. Gutzwille, Phys. Rev. B **134A**, 923 (1964); M.C. Gutzwille, Phys. Rev. B **137A**, 1726 (1965)
16. F. Gebhard, Phys. Rev. B **41**, 9452 (1990)
17. F. Gebhard, Phys. Rev. B **44**, 992 (1991)
18. G. Kotliar, A.E. Ruckenstein, Phys. Rev. Lett. **57**, 1362 (1986)
19. W. Metzner, D. Vollhardt, Phys. Rev. Lett. **62**, 324 (1989)
20. A. Georges, G. Kotliar, W. Krauth, M. Rozenberg, Rev. Mod. Phys. **68**, 13 (1996)
21. M.M. Korshunov, V.A. Gavrichkov, S.G. Ovchinnikov, I.A. Nekrasov, Z.V. Pchelkina, V.I. Anisimov, Phys. Rev. B **72**, 165104 (2005)
22. S.G. Ovchinnikov, I.S. Sandalov, Physica C **161**, 607 (1989)
23. V.A. Gavrichkov, S.G. Ovchinnikov, A.A. Borisov, E.G. Goryachev, Zh. Eksp. Teor. Fiz. **118**, 422 (2000) [JETP **91**, 369 (2000)]; V. Gavrichkov, A. Borisov, S.G. Ovchinnikov, Phys. Rev. B **64**, 235124 (2001)
24. M.M. Korshunov, S.G. Ovchinnikov, A.V. Sherman, Phys. Met. Metallogr. **101**, Suppl. 1, S6 (2006)
25. J.C. Hubbard, Proc. Roy. Soc. London A **277**, 237 (1964)
26. R.O. Zaitsev, Sov. Phys. JETP **41**, 100 (1975)
27. Yu. Izumov, B.M. Letfullov, J. Phys.: Condens. Matter **3**, 5373 (1991)
28. S.G. Ovchinnikov, V.V. Val'kov, *Hubbard Operators in the Theory of Strongly Correlated Electrons* (Imperial College Press, London, 2004)
29. J.C. Hubbard, Proc. Roy. Soc. London A **276**, 238 (1963)
30. N.M. Plakida, V.Yu. Yushankhai, I.V. Stasyuk, Physica C **162–164**, 787 (1989)
31. S.G. Ovchinnikov, E.I. Shneyder, Central European J. Phys. **3**, 421 (2003)
32. C. Grober, R. Eder, W. Hanke, Phys. Rev. B **62**, 4336 (2000)
33. V.V. Val'kov, D.M. Dzebisashvili, Zh. Eksp. Teor. Fiz. **127**, 686 (2005) [JETP **100**, 608 (2005)]
34. H. Shimahara, S. Takada, J. Phys. Soc. Jpn **60**, 2394 (1991); H. Shimahara, S. Takada, J. Phys. Soc. Jpn **61**, 989 (1992)
35. A. Barabanov, O. Starykh, J. Phys. Soc. Jpn **61**, 704 (1992); A. Barabanov,V. M. Berezovsky, Zh. Eksp. Teor. Fiz. **106**, 1156 (1994) [JETP **79**, 627 (1994)]
36. A. Sherman, M. Schreiber, Phys. Rev. B **65**, 134520 (2002)
37. A.A. Vladimirov, D. Ile, N.M. Plakida, Theor. i Mat. Fiz. **145**, 240 (2005) [Theor and Meth. Physics **145**, 1575 (2005)]
38. V.V. Val'kov, T.A. Val'kova, D.M. Dzebisashvili, S.G. Ovchinnikov, Pis'ma v ZhETF **75**, 450 (2002) [JETP Lett. **75**, 278 (2002)]
39. M.M. Korshunov, S.G. Ovchinnikov, A.V. Sherman, Pis'ma v ZhETF **80**, 45 (2004) [JETP Lett. **80**, 39 (2004)]
40. I.M. Lifshitz, Sov. Phys. JETP **11**, 1130 (1960)
41. G.E. Volovik, Acta Phys. Slov. **56**, 49 (2006); e-print `arXiv:cond-mat/0601372`
42. N.M. Plakida, V.S. Oudovenko, Physica C, doi: 10.1016/j.physc.2007.03.410 (2007)
43. N.M. Plakida, V.S. Oudovenko, Zh. Eksp. Teor. Fiz. **131**, 259 (2007) [JETP **104**, 230 (2007)]
44. T. Tohyama, Phys. Rev. B **70**, 174517 (2004)